PAPER

# Brain-controlled cycling system for rehabilitation following paraplegia with delay-time prediction

# Brain-controlled cycling system for rehabilitation following paraplegia with delay-time prediction

Shintaro Nakatani[1], Nozomu Araki[2], Takayuki Hoshino[3], Osamu Fukayama[4], and Kunihiko Mabuchi[5]

Email: snakatani@tottori-u.ac.jp

1 School of engineering, Tottori University
snakatani@tottori-u.ac.jp
2 Graduate School of Engineering, University of Hyogo
araki@eng.u-hyogo.ac.jp
3 Graduate School of Science and Technology, Hirosaki University
thoshino@hirosaki-u.ac.jp
4 Center for Information and Neural Networks, National Institute of Information and Communications Technology
o.fukayama@nict.go.jp
5 Graduate School of Information Science and Technology, the University of Tokyo
Kunihiko_Mabuchi@ipc.i.u-tokyo.ac.jp

## Abstract

***Objective:*** Robotic rehabilitation systems have been investigated to assist with motor dysfunction recovery in patients with lower-extremity paralysis caused by central nervous system lesions. These systems are intended to provide appropriate sensory feedback associated with locomotion. Appropriate feedback is thought to cause synchronous neuron firing, resulting in the recovery of function.
***Approach:*** In this study, we designed and evaluated an ergometric cycling wheelchair, with a brain-machine interface (BMI), that can force the legs to move by including normal stepping speeds and quick responses. Experiments were conducted in five healthy subjects and one patient with spinal cord injury (SCI), who experienced the complete paralysis of the lower limbs. Event-related desynchronization (ERD) in the β band (18-28 Hz) was used to detect lower-limb motor images.
***Main results:*** An ergometer-based BMI system was able to safely and easily force patients to perform leg movements, at a rate of approximately 1.6 seconds/step (19 rpm), with an online accuracy rate of 73.1% for the SCI participant. Mean detection time from the cue to pedaling onset was 0.83±0.31 s.
***Significance:*** This system can easily and safely maintain a normal walking speed during the experiment and be designed to accommodate the expected delay between the intentional onset and physical movement, to achieve rehabilitation effects for each participant. Similar BMI systems, implemented with rehabilitation systems, may be applicable to a wide range of patients.

**keywords**: brain–machine interface, event related desynchronization, ergometer, self-agency

## Introduction

Huge efforts have been invested in robotic rehabilitation that uses electroencephalography (EEG) to create a brain-machine interface (BMI) (1,2). These robots are used to facilitate physiotherapeutic treatments for stroke and spinal cord injury (SCI) patients, and the control signal that activates the robots depends on the movement intention obtained through the BMI (3,4). Several studies have reported combining robotic rehabilitation and functional electrical stimulation (FES) with BMI to recover upper- and lower-limb function in stroke (5,6) and SCI patients (7,8). The synchronization between the motor imagery and somatosensory cortex stimulation is thought to enhance the long-term recovery of locomotion compared with continuous spinal cord stimulation, based on experimental evidence in SCI rat models (9) and humans (10).

Neuroplasticity, caused by synchronous firing, is the key to functional recovery. Spike-timing dependent plasticity (STDP) is a temporally asymmetric form of Hebbian learning, induced by temporal correlations between the spikes of pre- and post-synaptic neurons (11,12). During STDP, when neurons fire causally, the connectivity increases; however, when neurons fire anti-causally, the connectivity decreases. Moreover, neuronal plasticity relies on how closely the pre- and post-synaptic neurons fire with respect to time. Hence, synchronous firing, which is both causal and close in time, is an important feature of a robotic rehabilitation system that aims to enhance the long-term recovery of locomotion. Robotic-assisted gait training can provide signal-level proprioceptive feedback during clinical use (13,14). Normal gait speed induces higher amplitudes of electromyography (EMG) bursts in various muscles. Beres-Jones and Harkema reported that the effects on EMG amplitude and burst duration were similar between complete and incomplete SCI patients when using body weight support on a treadmill (15). Therefore, rehabilitative strategies designed to provide appropriate sensory feedback associated with locomotion, including normal stepping speeds and maximized loading on the legs, are important for triggering the synchronous firing of neurons.

Robotic exoskeletons for SCI patients have been reported previously, featuring balance control (16,17), weight-supported systems, and FES (18,19). These studies have generally focused on the construction of closed-loop walking exoskeletons guided by the intentions of the patients. Selfslagh et al. proposed the walk-again neuro-rehabilitation protocol, which observed cardiovascular improvements and less dependency on walking assistance, but also partial neurological recovery in complete SCI patients and reported that the preferred speed improved from 8 s/step to 3 s/step during the rehabilitation protocol (20). By using weight-suspended systems with a treadmill, such as the Lokomat (Hocoma Medical Engineering Inc, Zurich, Switzerland), the protocol can easily set both stepping speeds and the loading of the legs(20). However, these devices have been reported with some difficulties during rehabilitation. The

Lokomat reduces the load on the legs by standing the patient upright and suspending the patient, using a safety belt, which is associated with safety risks and requires the support of several persons. Furthermore, no visual feedback is associated with displacement because the patient is on a treadmill during rehabilitation. Lopez et al. reported a protocol involving exoskeleton systems and parallel bars, with special considerations, such as safety, timing, and the control of patients' fatigue levels (21). They reported that "one gait cycle can be completed within 6 seconds (3 s/step)". However, the recruited patients were incomplete SCI patients who maintained certain balance control, and the system required a complex set-up and additional safety measures to avoid falls; therefore, the gait speed and the loading on the legs were not points of focus. Normal gait speeds and loading the legs contribute to proprioceptive and tactile feedback, which cause synchronous firing in the central nervous systems. Thus, designing a system that can maintain a normal gait speed both easily and safely during experiments remains important for increasing the clinical application of robotic BMI rehabilitation systems.

In this study, we investigate the feasibility of a system designed to provide normal gait training using a cycling wheelchair (22,23), driven by ergometric movements. Ergometer cycling offers training characteristics that include the advantages of muscle coordination (24,25). A cycling wheelchair can provide sufficient kinetic strength to activate the reflex network, by forcing the pedals to rotate, while simultaneously providing mobility, by moving the wheelchair forward. Furthermore, moving the patient from a wheelchair to the system can be performed both easily and safely. First, we proposed an ergometer-type of robotic device and classifier. The classification protocol for detecting the motor intentions of patients, both accurately and quickly, plays a key role in synchronizing the intention to move with the proprioceptive feedback (26). In our implementation, the model takes the form of an autoregressive (AR) model, whose innovation term is obtained by the linear combination of EEG power spectrum densities (PSDs), obtained using a sliding window approach. Second, we evaluated the performance of the classifier for discriminating between rest and actual movement (in healthy patients) or leg motor imagery (in an SCI patient). The achievement of normal stepping speeds and rapid responses by the ergometer system represents a necessary step toward increasing the clinical applications of BMI rehabilitation systems and implies the feasibility of using synchronous firing to enforce STDP for functional recovery.

## Brain controlled cycling systems

### *Cycling wheelchair system*

Figure 1 (a) shows a conceptual image of a cycling wheelchair system, based on BMI. A commercial cycling wheelchair (Profhand, TESS, Sendai, Japan) was equipped with a direct current (DC) motor and

disc brakes, for driving and steering the wheelchair. The drive wheels are linked to the pedal axle. Patients can safely maintain a normal gait speed (>3 s/step) and be provided with visual feedback through displacement during rehabilitation. The rudder was controlled so that the wheelchair travels around a circle of a certain diameter. Signal processing and motion control are performed by a laptop computer on the system.

### *Ergometer system*

An ergometer-type BMI system was developed for the experiment. This system, unlike the wheelchair system, cannot be maneuvered; however, with a simple set-up, the lower extremities of the patient can be moved at a normal speed, as shown in Figure 1 (b). An ankle-foot orthosis (AFO) (Ortop AFO, Pacific Supply, Osaka, Japan) was attached to each pedal, allowing the patient to pedal without touching the ground even if the patient is a foot drop. When the system detects the patient's intention to pedal, a DC motor (RE40, Maxon motor ag., Sachseln, Switzerland) attached to the shaft forces the pedals, cranks, and the paralyzed lower extremities to move. The rotation ratio between the pedal shaft and the driving motor was 1:25. All experiments in this study were measured using this system.

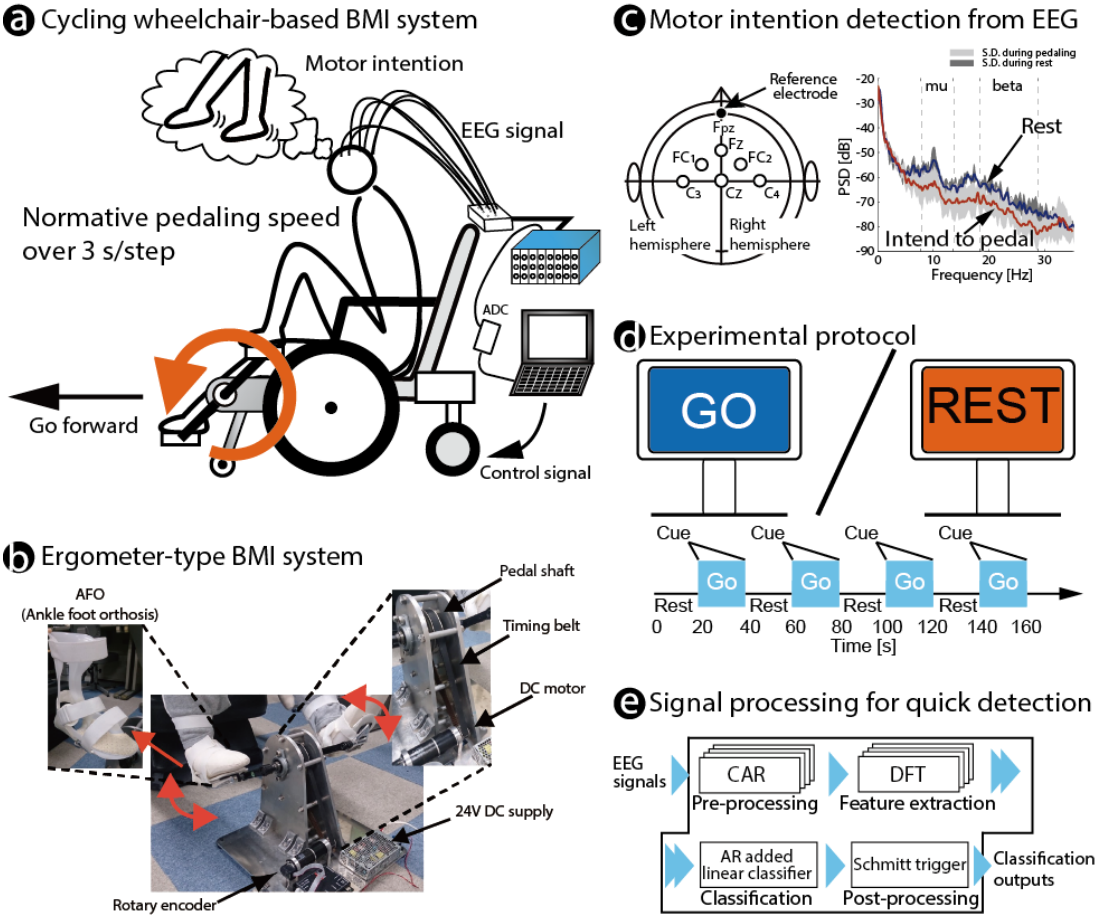


**Figure 1. Overview of the proposed system and the experimental design. (a) Cycling wheelchair-based BMI system for the rehabilitation of patients with SCI and lower-extremity paralysis. An SCI patient sits on the wheelchair, with the legs fixed on the pedals by braces. All components, including a battery, a laptop PC, an amplifier and ADC and a wheelchair control unit, were placed on the wheelchair. (b) Ergometer-type BMI system for the rehabilitation of patients with SCI and lower-extremity paralysis. (c) Electrode positions and the comparison of PSDs between rest (blue) and pedaling intention (red) at the Cz electrode of P1 (mean ±SD). (d) Experimental protocol. (e) Schematic diagram of the proposed classifier.**

## Methods

### *Participants* recruitment

Five healthy males (referred to as H1–H5), aged 63, 22, 23, 21 and 22 years old (H1 is an author), and one male SCI patient (referred to as P1), aged 53 years old, were enrolled in this study. P1 suffered a traumatic SCI at the spinal T3 vertebral level, with complete paraplegia of the lower extremities, due to a traffic accident in 1999. Informed consent was obtained from all participants

before the experiments. The experimental design details were approved by the ethics committees of the University of Tokyo (13-107).

*Data acquisition*

As shown in Figure 1 (c), EEG signals were recorded from six NE-121J working electrodes (Nihon Kohden Corp., Tokyo, Japan), located at the Cz, C3, C4, FC1, FC2, and Fz positions, based on the international 10/20 system, and one reference electrode was placed at the forehead (Fpz). The working electrode positions covered the premotor, motor, and somatosensory areas. All electrodes were fixed to the scalp, using a Z-181JE conductive EEG paste (Nihon Kohden Corp., Tokyo, Japan). EEG signals were amplified 100,000-fold, and a 0.5-Hz high-pass filter and a 300-Hz low-pass filter were applied, using an AB-611J biosignal amplifier (Nihon Kohden Corp., Tokyo, Japan). The EEG signals were recorded using an NI USB-6211 data acquisition device (National Instruments Corp., TX, USA), at a sampling rate of 1 kHz. All impedances between the reference electrode and each working electrode were under 10 kΩ.

As shown in Figure 1 (d), which illustrates the mean of the PSD amplitudes of P1 measured at the Cz electrode, PSDs during motor intention around the μ (8–13 Hz) and β (18–28 Hz) bands decreased more compared with the resting period. The β-band PSDs decrease (desynchronize) in the parietal area when a participant intends to move his or her foot is well known as β-band Event-related desynchronization (ERD)(27,28). Therefore, we used β-band ERD as features for the detection of the pedaling movement itself and the intention of pedaling.

We were concerned that the measured EEG signals had been corrupted by EMG. There are methods for detecting such corruption using different features, for example, placing a large number of electrodes on the head with high-density and interpolating them using the information of the surrounding electrodes (29,30). Only six electrodes were measured in this paper, and this has the advantage of shortening the preparation time of EEG measurement but presents difficulty in terms of its application to the above methods. Therefore, we used a single-channel method (31,32) to detect potential corruption, which focuses on the shape of frequency spectra. In this study, we used the slope of the spectrum in the 5–70 Hz range of the EEGs. The measured EEG signals were analyzed every second using the 250-order Burg method with 1,000 data points and no overlap. When the slope was −0.3 dB/Hz or more, we defined as having been corrupted. The contamination ratio, which was obtained by dividing the number of corrupted datasets by the number of evaluated datasets, was 0% for H1, H3, and H4. The maximum corruption ratios were 1.9% (3 and 5 ch) for H2, 2.2% (3 ch)

for H5, and 0.65% (2 ch) for P1. We decided that these values were sufficiently low to indicate that the results of this paper were not the result of data corruption.

*Experimental procedure*

We recorded EEG signals for H1–H5 during pedaling and resting. One EEG recording lasted 160 s, and the trial included four 40 s repetitions of the task (20 s pedaling followed by 20 s rest as shown in Figure 1(d)). Participant 1 opted to pedal instead of a motion. The required number of trials (eight) was obtained by statistical power analysis of a two-sided t-test at the desired power level of 0.8, a significance level of 0.05, a mean accuracy difference of 15%, and a standard deviation of 10%. We set hypothetical values for the deviation and difference of mean accuracy based on Wang (33). Thus, we executed two trials for the 160 s test for each participant to derive the EEGs for eight trials. Shortening the duration of each trial is also advantageous for preventing a decrease in classification performance as relearning using the preceding trial can easily be achieved. The cue for each pedaling or rest period was an audible beep. Here, H1–H5 performed the task at a speed of 30 rpm. Each participant closed their eyes during the recording.

P1 sat on a wheelchair and attached his feet and ankles to the pedals, using the AFO. We asked P1 to visualize riding a bicycle up a slope. After the task, we confirmed whether he was able to successfully visualize pedaling up a slope.

*Signal processing and classification*

Figure 1 (e) shows a schematic diagram of the proposed method for classifying signals. The six EEG signals recorded for each participant were applied to a common average reference (CAR; explained later in the Signal Preprocessing section). CAR is a common method used to remove the effects of the reference electrode EEG (33,34) and electrocorticography (ECoG) (35). ERD signals were obtained for feature extraction, using discrete Fourier transform (DFT). These features were used for classification, using the proposed classifier. Finally, for post-processing, we applied the dual-threshold method (36), to reduce short-term detection errors. This dual-threshold method is also called the “Schmitt trigger gate” in the field of electronic engineering. A Schmitt trigger gate is a binary classifier with two thresholds, $T_1, T_2$ ($T_1 \geq T_2$), and the final classification output through the Schmitt trigger gate, $y'(t)$, is given as

$$y'(t) = \begin{cases} +1, & \text{if } y(t) \geq T_1 \\ -1, & \text{if } y(t) \leq T_2 \\ y'(t-1), & \text{otherwise} \end{cases}.$$

We set the dual thresholds as $T_1 = 0.3$ and $T_2 = 0$ and the initial output as $y'(0) = -1$.

The EEG signals contained noise, derived from the reference electrode; for example, electromyogram, electrooculogram, and noise generated from changes in the impedance between the skin and each electrode. Therefore, during signal preprocessing, we applied a CAR to all EEG signals. A CAR is a process that subtracts the mean of all measured signals from each EEG signal, $e_k^{\mathrm{raw}}(t)$, at time $t$. The CAR-applied EEG signal, $e_i(t)$, is given as

$$e_i(t) = e_i^{\mathrm{raw}}(t) - \frac{1}{n}\sum_{k=1}^{n} e_k^{\mathrm{raw}}(t),$$

where $n$ is the number of working electrodes and $i \in \{1, \dots, n\}$.

The PSDs of the β band (18–28 Hz) were obtained to detect the leg movement or the intention to move (27,28), using the DFT of the CAR-applied EEG signals. The window length was 1000 ms (1000 points), and the overlap length was 900 ms (900 points).

We proposed a classifier that attaches the convolution term of the past output to a linear discriminant analysis (LDA) classifier. We described a method for obtaining the proposed classifier based on the recursive least squares method. We assumed that $x(t) \in \mathbb{R}^n$ denotes the feature vector, and $y(t) \in \{\text{Pedaling: } +1, \text{Rest: } -1\}$ denotes the task. Our proposed classifier is, therefore, given as

$$y(t) = \sum_{i=1}^{n} x_i(t) \cdot a_i + \sum_{j=1}^{m} y(t-j) \cdot b_j \tag{1}$$

$$= \mathbf{z}^{\top}(t)\mathbf{w}, \tag{2}$$

where $b_j$, $j = 1, \cdots, m$ is the coefficient of an AR term. $\mathbf{w} = [a_1, \cdots, a_n, b_1, \cdots, b_m]^{\top} \in \mathbb{R}^{n+m}$ and $\mathbf{z}(t) \in \mathbb{R}^{n+m}$ are the vectors that construct the features. In this experiment, the number of working electrodes, $n$, was set to 6, and the number of AR terms, $m$, was set to 2. The time-variant coefficient, $\mathbf{z}(t)$, is expressed as

$$\mathbf{z}(t) = [x_1(t), \cdots, x_n(t), y(t-1), \cdots, y(t-m)]^{\top}.$$

The second term of equation (1) was considered as an infinite impulse response (IIR) filter. The weight vector, $\mathbf{w}$, was estimated from $\boldsymbol{z}(t)$ and $y(t)$ $(t = m, m+1, \dots, t_{\mathrm{end}})$. We obtained the estimated vector $\hat{\mathbf{w}}_t$ by using a Kalman filter $\hat{\boldsymbol{w}}$ $\left(= \hat{\boldsymbol{w}}_{t_{\mathrm{end}}|t_{\mathrm{end}}}\right)$, which was calculated as follows:

$$\widehat{\boldsymbol{w}}_{t|t-1} = \widehat{\boldsymbol{w}}_{t-1|t-1}$$

$$\widehat{\boldsymbol{P}}_{t|t-1} = \widehat{\boldsymbol{P}}_{t-1|t-1} + \boldsymbol{Q}$$

$$\boldsymbol{g}(t) = \frac{\widehat{\boldsymbol{P}}_{t|t-1}\boldsymbol{z}(t)}{\boldsymbol{z}^{\top}(t)\widehat{\boldsymbol{P}}_{t|t-1}\boldsymbol{z}(t) + R}$$

$$\widehat{\mathbf{w}}_{t|t} = \widehat{\mathbf{w}}_{t|t-1} + \boldsymbol{g}_t\left(y(t) - \mathbf{z}^{\top}(t)\widehat{\mathbf{w}}_{t|t-1}\right)$$

$$\widehat{\boldsymbol{P}}_{t|t} = \left(\boldsymbol{I} - \boldsymbol{g}(t)\boldsymbol{z}(t)\right)\widehat{\boldsymbol{P}}_{t|t-1}$$

where $\mathbf{P}_{t|t} \in \mathbb{R}^{(n+m)\times(n+m)}$ is the nonsingular matrix and $\boldsymbol{Q}$, and $R$ are the zero-mean Gaussian white noise, with covariance, of the process and the observation, respectively; in this study, $\boldsymbol{Q}$ was set to $\mathbf{0}$ and $R$ was set to 1.1. To obtain $\widehat{\boldsymbol{w}}$ from the recursive calculations of the equations, the initial values were set to $\hat{y}(-1) = \cdots = \hat{y}(-m) = 0, \mathbf{P}_0 = 10 \times \boldsymbol{I},$ and $\widehat{\boldsymbol{w}}_0 = \mathbf{0}$, respectively, where $\boldsymbol{I}$ is an identity matrix of an appropriate size.

*Classification accuracy evaluation*

To evaluate the classification accuracy of the pedaling movement/intention in H1–H5 and P1, we defined the classification rate as:

$$\text{Accuracy rate} = \frac{\text{Number of correct datasets}}{\text{Number of discriminated datasets}} \times 100\ [\%].$$

We took 37-s data clips, from 17 s before the cue to 20 s after the cue, during each experiment when conducting offline classification. To focus on the delay time at the onset of pedaling, the first 3 s of the rest period, which may have been affected by stopping pedaling, were excluded from the evaluation. All participants recorded two trials per experiment. Accordingly, eight data clips were used for the classification of the performance evaluation. We applied eight-fold cross-validation to obtain the error rate. Additionally, the two performance measures below were employed to obtain the normalized confusion matrix:

$$\text{True rest rate} = \frac{\text{Number of correct rest datasets}}{\text{Number of rest datasets}},$$

$$\text{True pedaling rate} = \frac{\text{Number of correct datasets classified as pedaling}}{\text{Number of pedaling datasets}}.$$

*Selecting the trade-off between the delay time and accuracy of classifier results*

Recent studies on neuroplasticity for long-term recovery suggest the importance of shorter delay times and the more accurate detection of motor images during BMI rehabilitation. Although a trade-off exists between the detection delay time associated with motor imagery and the accuracy of classification, the delay time during BMI rehabilitation has not been thoroughly discussed in existing studies. The bulk of studies have evaluated discrimination performance by distinguishing between "exercise trial" and "exercise periods" to assess the performance of online classification (20,21,37). In these cases, participants imagined their movements during the "movement attempt" period, and the BMI rehabilitation system drove participants' legs during the "movement" period, evading artifacts from the exoskeletal apparatus by avoiding the simultaneous performance of EEG measurements and device movements. However, our protocol classifies the movements and images every 100 ms during the ergometer experiment without a "movement attempt" period, and this is because few artifacts are associated with ergometer movements. Moreover, in our proposed classifier, parameter m in equation (1) can be used to select the trade-off between the delay time and accuracy. We describe the guidelines used to select parameter $m$.

## Results

### *Offline classification performance*

Figure 2 shows the mean error rate of all participants. The error rates for H1–H5 were 14.5±3.1%, 21.8±8.9%, 14.5±11.7%, 18.1±13.9%, and 25.5±9.3%, and the mean was 18.7% (broken line), whereas the mean error rate for P1 was 27.1±7.7%. The error bars show the standard deviations of the eight data clips for each participant. The confidence interval for the mean accuracy of the healthy participants was 13.7%–24.7%. All error rates were lower than the chance level (50%). The mean error rate of P1 was not different from that of healthy participants (H1-H5). Figure 3 shows confusion matrix for healthy subjects (H1-H5) and SCI participants (P1). The true rest rate was 0.77 for the healthy subjects and 0.74 for the SCI participant, and these looks similar. The accuracy rate during true pedaling was 0.84 for the healthy participants, and it is higher than that of 0.72 for the SCI participant. In the previous system, trial periods were set so that only one classification result was obtained for each period. The accuracy rates reported by Lopez et al., which detected the trigger during movement attempt periods, 3 s after the previous period, were 68%–97% (healthy participants) and 18.8%–100% (SCI patient) (21). Wang et al., who classified based on every 4 s of data, reported accuracy rates of 75.1% (healthy participants) and 94.5% (SCI patient) (37). Selfslagh et al., who classified using a movement attempt period of 3.75 s after a cue period of 1.25 s, reported accuracy rates of 73.9% ± 3.6% and 83.2% ± 8.2% in two SCI patients) (20). As mentioned above, these studies assessed the accuracy rate of the

classification results for the trial period. In the present study, the error rate was comparable to these studies, even though the classification of this protocol was always performed during the pedaling exercise.

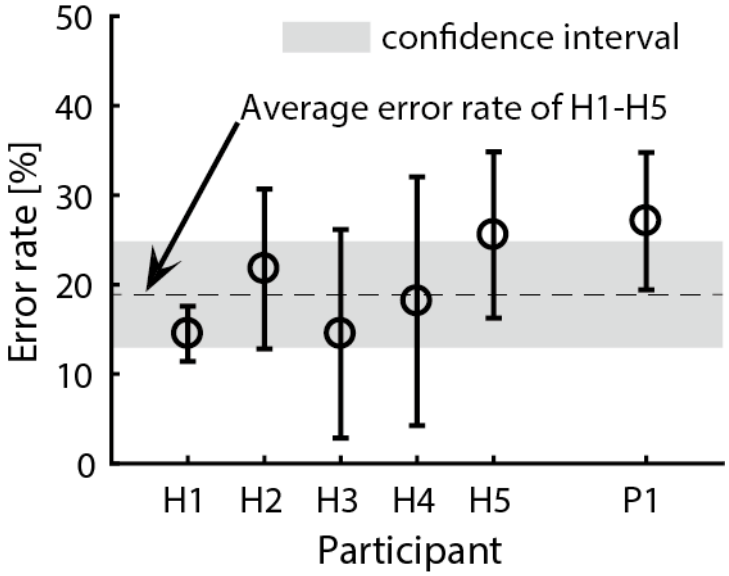


**Figure 2. Means of the error rates for healthy participants (H1–H5) and the SCI patient (P1). Error bar: the SD gray area shows the confidence interval (95%) for H1–H5.**

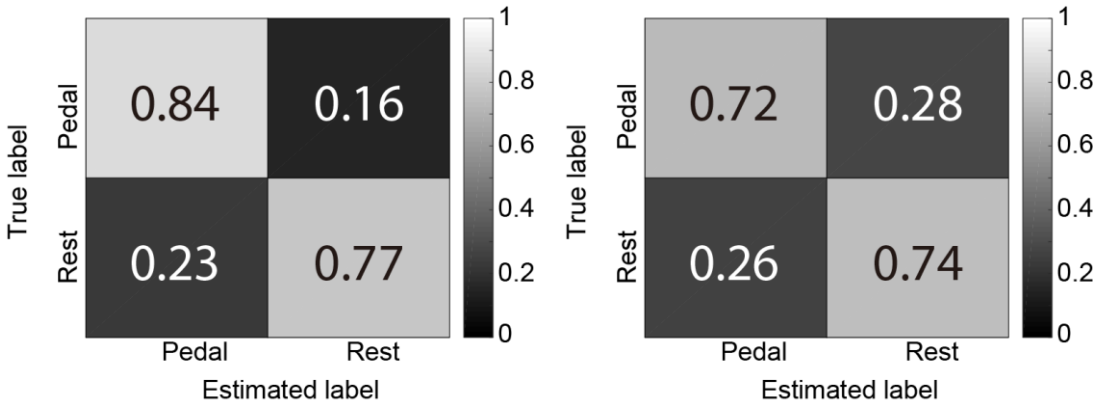


(a) Healthy participants (H1–H5) (b) SCI participant (P1)

**Figure 3. Normalized confusion matrices of (a) the healthy participants (H1-H4) and (b) the SCI participant (P1). The true rest was 0.77 in the healthy participants and 0.74 in the SCI participant. The accuracy rate during true pedaling was 0.84 for healthy participants and 0.72 for the SCI participant.**

*Parameter settings*

Figure 4 shows the mean error rates of H1–H5 when the parameter $m$ increased from zero to nine; error bars show the standard errors. The accuracy rates of the proposed method (when $m$ was greater than zero) were better than those using the common LDA method (when $m$ was equal to zero). The mean error rate fell under 15% when the parameter $m$ was nine. This figure suggests that the parameter $m$ should be increased if the engineer wants to decrease the error rate.

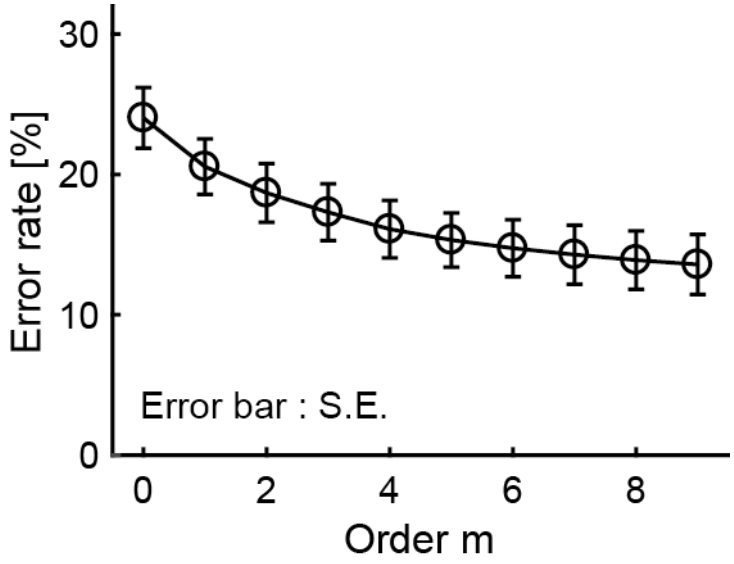


**Figure 4. Accuracy rates as the order of the AR terms. Means of the five healthy participants (H1–H5). The error rates were obtained from eight-fold cross-validation in offline processing and a learning effect was canceled.**

The short delay between starting the motor intention and the actual movement of the body is important for the realization of neuronal connectivity. The sense of agency and the experience of controlling our actions requires that action-related and effect-related signals be integrated within a time window (38). In an experiment during which visual feedback was performed after a certain delay after button pressing, the degree to which participants felt that they were controlling the visual feedback decreased with increasing delay time. A delay time shorter than 334 $\pm$ 27 ms from the time of that movement occurred was able to make the majority of participants feel as though they were in full control; however, the majority of participants felt that a delay of more than 708 $\pm$ 42 ms indicated that they had no control. When a 1-second "move attempt" period exists, self-agency has been difficult to generate in previous studies. In this study, the proposed classifier was able to classify the pedaling imagery, without a “movement attempt” period, and can adjust the trade-off between accuracy and quick response by selecting the parameter $m$.

The delay time was defined as the time from the movement onset to the time that the sign of the classifier switches from negative to positive. The delay in this experiment can be separated into a participant-based cognitive and operational delay and a BMI-based delay associated with the EEG measurements and classifiers. Table 1 shows the delay times of healthy participants from the cue to the onset of pedaling. The mean delay times of H1 and H2 were both 500 ms, but those of H3, H4, and H5 were approximately 1,000 ms. These results suggest that individual differences exist in the delay time. The delay time based on the BMI system represents the time from the start of pedaling to the time when the classification output switched to positive. Figure 5 shows the mean outputs of the classifier, at the parameters $m =$ 0, 2, and 6, for H4. The delay time based cognitive and operational delay was 0.8 s. Thus, the mean delay times, based on the BMI at $m =$ 0, 2, 6, were $-0.04$ s, 0.27 s, and 0.51 s, respectively. Based on Figure 5, parameter $m$ should be decreased if the operator desires to decrease the delay time.

**Table 1. Mean delay time of each participant. The time between from the cue signal is indicated and to the subject begins to move the pedal, includes the cognitive and operational delay, and based on the motor ability of the participants.**

| Subject ID | Delay time mean±std [ms] |
|---|---|
| H1 | $500 \pm 13$ |
| H2 | $500 \pm 5$ |
| H3 | $1000 \pm 11$ |
| H4 | $990 \pm 23$ |
| H5 | $1180 \pm 23$ |

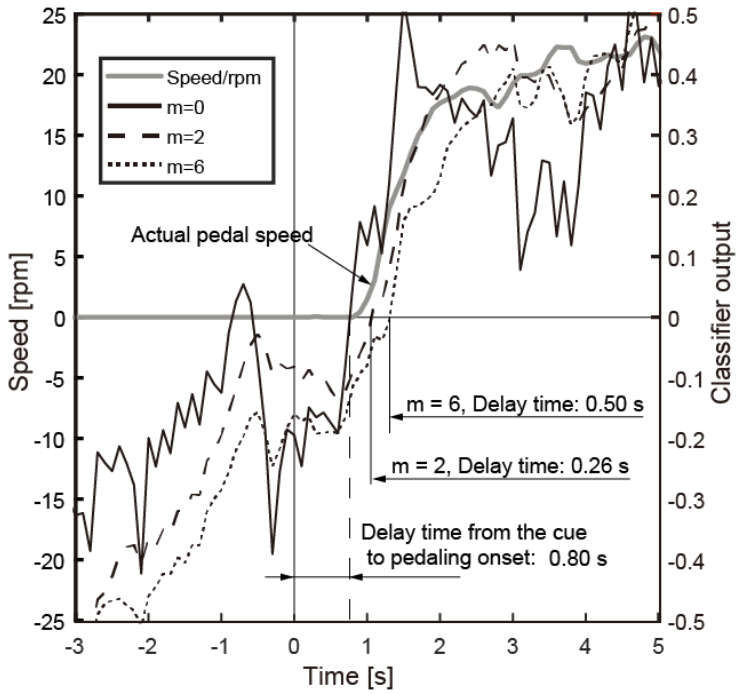


**Figure 5. Arithmetic means of the output values around the increasing time delay.**

Other research that has investigated walking movements, using auditory feedback combined with moving step (39). The relationship between the time delay and self-agency changes periodically because the participants can feel the synchronization between the legs and the auditory stimulation not only during the present step but also from the previous step. However, that study focused on walking at a constant speed and did not focus on the initiation of walking. In this study, rapid detection was given priority over the leg angle (phase) matching. Therefore, we only need to focus on the quick and accurate detection of movement in this system.

Therefore, we can select the parameter $m$ automatically, using the below steps:

1. Decide the acceptable delay time
2. Calculate the mean delay time and decide the range of parameter $m$ that can satisfy the acceptable delay time
3. Calculate the error rate and then select the value for parameter $m$ that minimizes the error rate from the decided range

Figure 6 illustrates the relationship between the delay times and accuracy rates of H4 and P1. Here, 0 ms indicates the cue to the participant, and 990 ms is when the pedal movement occurs following the intention to do so (see Table 1). Parameter “m” can be set to 5 if the expected delay time is set to $990 + 334$ ms as shown in Figure 6 (a). On the basis of the results of the experiment in (34), the value required for the majority of the subjects to experience self-agency was denoted as 334 ms, and the value at which the majority of the participants did not experience self-agency was denoted as 704 ms. Because a delay time based on recognition could not be determined for P1, the mean delay time for H1–H4 (840 ms) was used. The optimal parameter $m$ value was set to 2 because the accuracy rates were identical between $m$ equals 2 and $m$ equals 3, if the expected delay time was set to $840 + 334$ ms in Figure 6 (b). According to these results, the expected delay time was shorter than the acceptable delay time, and the system performance can be controlled to achieve a rehabilitation effect in each participant. The optimal value of $m$ change from day to day if there is the learning effect, and $m$ will be changed by re-learning.

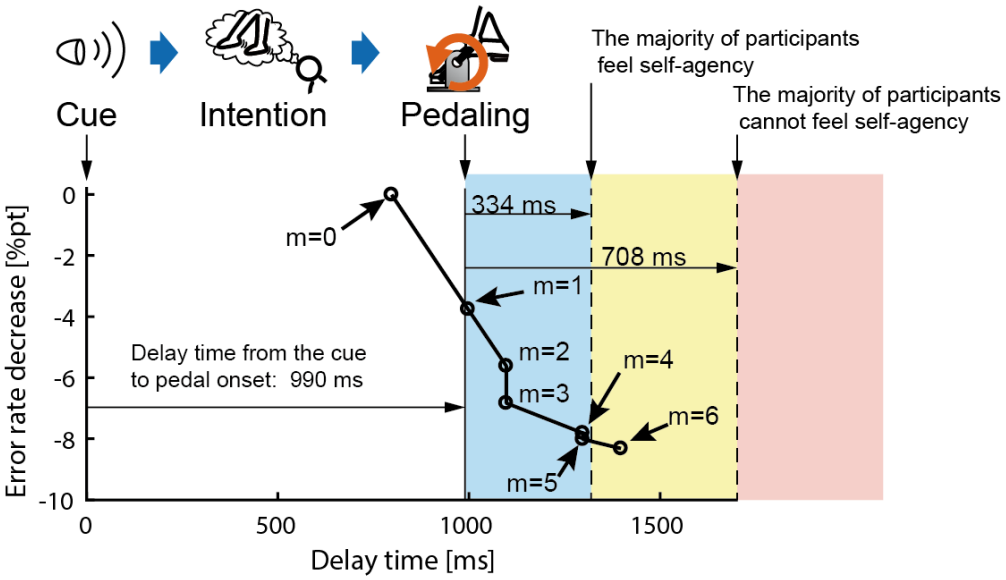


(a) Healthy participant (H4)

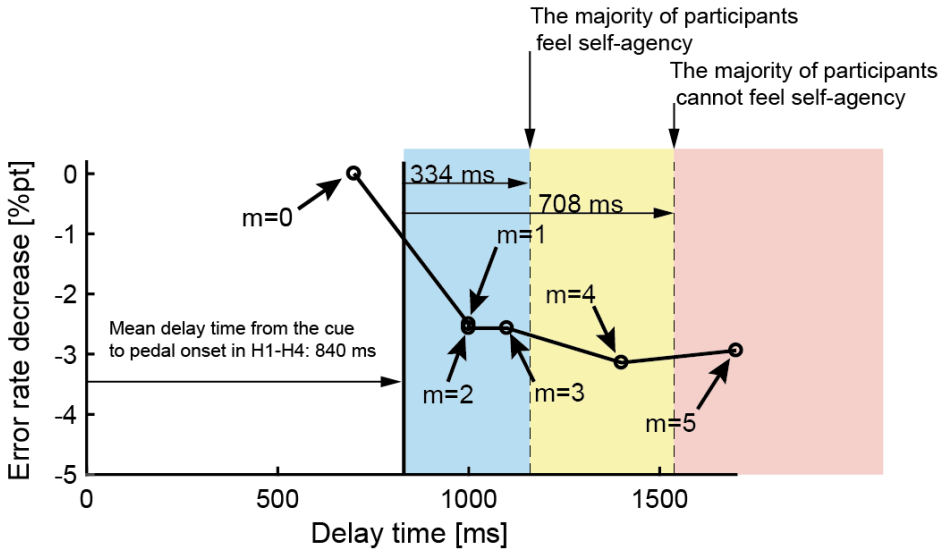


(b) SCI participant (P1)

**Figure 6. Relationships between accuracy rates and delay time at each AR order: (a) delay time is obtained from the mean of the cue to the onset of pedaling for H4 (see Table 1). It includes recognition time of the audible beep and the delay between intention to pedal and subsequent movement; (b) expected delay time was obtained from the mean of the cue to the onset of pedaling in H1–H5.**

*Online classification performance*

Figure 7 shows the results of the pedaling state detection for H3. Trial 1 was used to obtain learning data and trial 2 was used for online classification. Parameter $m$ was set as 2. Figure 7 (a) shows the 18-28 Hz band-pass-filtered EEG signal, measured at the Cz electrode, and Figure 7 (b) shows changes in the β-band PSD at the Cz electrode. The β band PSD amplitudes decreased when H3 was pedaling. Figure 7 (c) shows the classifier outputs calculated from Equation (2), and figure 7 (d) shows the post-processing detection results. The post-processing detection accuracy rate was 77.3%, and the error rate of the 160-s data was 22.7%. No difference in error rate was observed between online and offline experiments.

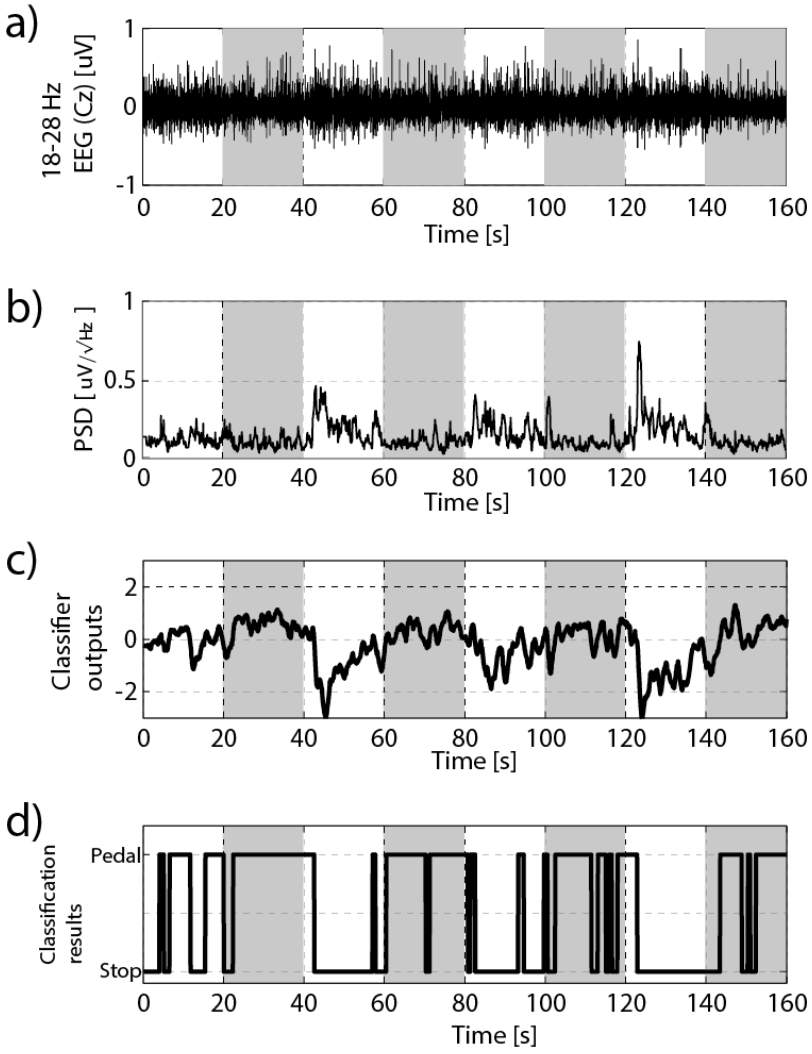


**Figure 7. Real-time motion estimation results for the healthy participant (H3)**
Shaded areas indicate the pedaling period. a) 18–28 Hz band-pass-filtered signal recorded at the Cz electrode. b) β band PSD at the Cz electrode. c) Outputs of the proposed classifier. d) Post-processing detection value. PSD, power spectrum density.

The ergometer-type BMI system performed forced rotations of the lower extremities and was synchronized with the detected movement intention. As shown in Figure 8, P1's lower extremities were attached to the pedals and forcibly rotated by the ergometer-type BMI system in synchronization with the classifier outputs. Figure 9 shows the detection results for the motor intention and forced rotation of P1's lower extremities. Parameter $m$ was set as 2. Shaded areas indicate periods during which we instructed P1 to try to move his lower extremities. Figure 9 (a) shows the 18-28 Hz band-pass-filtered EEG signal, measured at the Cz electrode. No specific motion artifacts were observed in the EEG signals. Figure 9 (b) shows changes in the β-band PSD at the Cz electrode. The amplitudes were relatively larger during the resting period compared with those during the motor intention period. Figure 9 (c) shows the classifier output, calculated from Equation (2), and Figure 9 (d) shows the post-processing detection results. In this experiment, the accuracy rate of the motor intentions was 73.1%. No difference in the error rate was observed between online and offline experiments. Figure 9 (e) shows the actual ergometer speed. The rotation speed was controlled to be 19 rpm.


**Figure 8. Experimental setup of the BMI-based forced lower-extremity rotation**

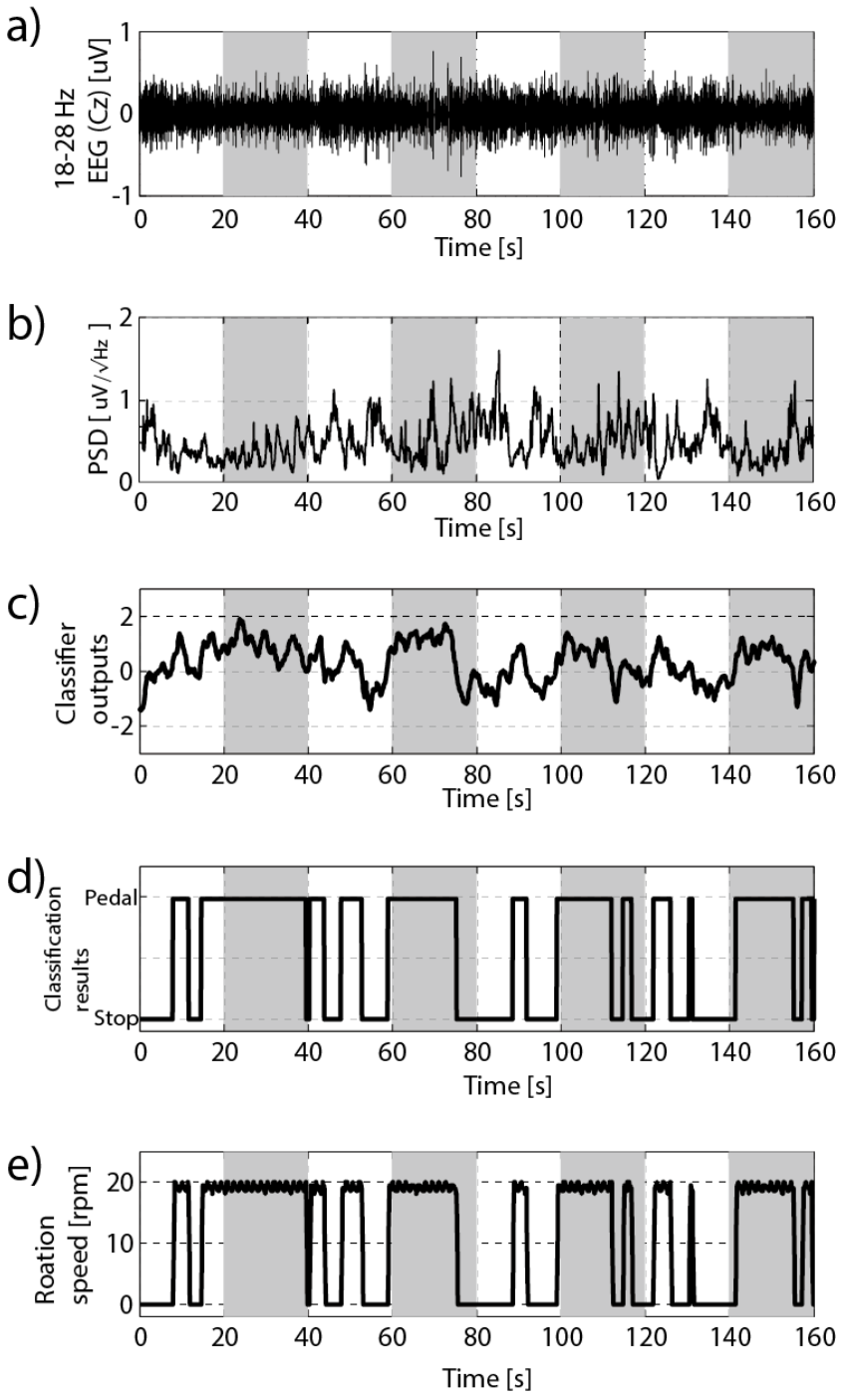


**Figure 9. Real-time experimental results for the ergometer-type BMI system for the patient with SCI (P1)**

Shaded areas indicate the pedaling intention period. a) 18–28 Hz band-pass-filtered signal recorded at the Cz electrode. b) PSD of the β band at the Cz electrode. c) Outputs of the proposed classifier. d) Post-processing detection value. e) Actual lower-extremity rotation speed during the real-time experiment was set to be 19 rpm (1.6 s/ step). SCI, spinal cord injury; PSD, power spectrum density.

## Discussion and conclusion

The mu band (around 10 Hz) PSD has been commonly used to detect a person's motor intention because the μ band has a higher amplitude compared with other high-frequency bands. However, we only used the β-band PSD for the detection of the intention to pedal, for the following reasons:

- β-band ERD is more related to movement tasks, especially of the legs, compared with the μ-band ERD (40,41).
- The μ-band ERD can be controlled using visual feedback training. Bhattacharyya et al. developed a co-adaptive BMI system that enables adaptive learning between a user and a decoder(42). Therefore, μ power can be controlled without motor intention, which was not suitable for our objective.

EEG measurements using dry-type electrodes, without a conductive paste, and a wireless amplifier can shorten the set-up for rehabilitation. Some dry electrodes have already been developed for easy and stable measurements (43–46). For the practical applications of the robotic BMI system, it is desirable to realize that the dry EEG measurement that can stably measure a β-band signal.

One limitation of this paper is that the performance required for rehabilitation is unclear. In terms of the BMI-based EEG classification, however, the 30% error rate in this paper is acceptable. However, on several occasions, the concentration of the SCI participant was disrupted when the BMI rehabilitation system started the pedaling motion. We consider self-agency to be the key to maintaining concentration while the system moves. In this system, several performances may be linked to triggering self-agency, such as accuracy, the time delay, and the crank phase. In particular, shortening the delay time is essential for maintaining a patient's motivation and inducing a sense of self-agency. The relationship between the delay time and sense of self-agency/ownership was investigated using an illusion by employing visual and motor integration on a fake hand (47). A sense of self-agency/ownership arose when the delay time was less than 190 ms. By contrast, when the delay time was between 290 and 490 ms, only a sense of self-agency was experienced. Similarly, a time delay in BMI rehabilitation may have affected the sense of self-agency of the paralyzed legs. The time delay for BMI-based rehabilitation should be more frequently noted, particularly in clinical trials. The results of this study demonstrated a BMI rehabilitation approach that can define the expected delay time, using a pedaling wheelchair. First, to demonstrate the concept of the proposed system, an experimental electric ergometer, and a bicycle wheelchair system were developed. The ergometer-type robotic device, EEG measurement, feature extraction, and classifier used in the experiment were presented. Second, using β-band ERD as a feature, we developed a classifier for the accurate and rapid detection of the patients' movement intentions. Third, the performance of the classifier to discriminate between resting and actual exercise (healthy participants) and exercise images

(SCI patients) was demonstrated using both offline and online experiments. These results showed that the proposed system was able to classify intentions, even when the legs are moved at a rate of 19 rpm. Finally, a parameter determination method for defining the expected delay time was described. The system was able to easily and safely maintain a normal walking speed, in accordance with the wishes of the SCI patients.

## Acknowledgments

This study was funded by JSPS KAKENHI Grant Numbers 20246045, 14J00320, 16K21290 and JKA Grant Number 25-79.

## REFERENCES

1. Soekadar SR, Birbaumer N, Slutzky MW, Cohen LG. Brain-machine interfaces in neurorehabilitation of stroke. Neurobiol Dis. 2015;83:172–179.
2. Lebedev MA, Nicolelis MAL. Brain-machine interfaces: From basic science to neuroprostheses and neurorehabilitation. Physiol Rev. 2017;97(2):767–837.
3. Nicolelis MAL. Brain–machine interfaces to restore motor function and probe neural circuits. Nat Rev Neurosci. 2003;4(5):417–422.
4. Lazarou I, Nikolopoulos S, Petrantonakis PC, Kompatsiaris I, Tsolaki M. EEG-based brain–computer interfaces for communication and rehabilitation of people with motor impairment: A novel approach of the 21st century. Front Hum Neurosci. 2018;12.
5. Tariq M, Trivailo PM, Simic M. EEG-Based BCI Control schemes for lower-limb assistive-robots. Front Hum Neurosci. 2018;12:312.
6. Müller-Putz GR, Scherer R, Pfurtscheller G, Rupp R. EEG-based neuroprosthesis control: a step towards clinical practice. Neurosci Lett. 2005;382(1–2):169–174.
7. Bouton CE, Shaikhouni A, Annetta N V., Bockbrader MA, Friedenberg DA, Nielson DM, et al. Restoring cortical control of functional movement in a human with quadriplegia. Nature. 2016;533(7602):247–250.
8. Mushahwar VK, Guevremont L, Saigal R. Could cortical signals control intraspinal stimulators? A theoretical evaluation. IEEE Trans Neural Syst Rehabil Eng. 2006;14(2):198–201.
9. Bonizzato M, Pidpruzhnykova G, DiGiovanna J, Shkorbatova P, Pavlova N, Micera S, et al. Brain-controlled modulation of spinal circuits improves recovery from spinal cord injury. Nat Commun. 2018;9(1):1–14.
10. Shokur S, Donati ARC, Campos DSF, Gitti C, Bao G, Fischer D, et al. Training with brain-machine interfaces, visuotactile feedback and assisted locomotion improves sensorimotor, visceral, and psychological signs in chronic paraplegic patients. PLoS ONE. 2018;13:1–33
11. Kandel E, Schwartz J, Jessell T, Siegelbaum S, Hudspeth AJ. Principles of Neural Science, Fifth Edition. McGraw Hill Professional; 2012.
12. Bi G, Poo M. Synaptic Modification by Correlated Activity: Hebb's Postulate Revisited. Annu Rev Neurosci. 2001;24(1):139–166.

13. Dijkers MP, Akers KG, Galen SS, Patzer DE, Vu PT. Letter to the editor regarding "Clinical effectiveness and safety of powered exoskeletonassisted walking in patients with spinal cord injury: Systematic review with meta-analysis." Med Devices Evid Res. 2016;9:419–420.
14. Contreras-Vidal JL, Bhagat NA, Brantley J, Cruz-Garza JG, He Y, Manley Q, et al. Powered exoskeletons for bipedal locomotion after spinal cord injury. J Neural Eng. 2016;13(3):031001.
15. Beres-Jones JA, Harkema SJ. The human spinal cord interprets velocity-dependent afferent input during stepping. Brain. 2004;127(10):2232–2246.
16. Kilicarslan A, Prasad S, Grossman RG, Contreras-Vidal JL. High accuracy decoding of user intentions using EEG to control a lower-body exoskeleton. In: 2013 35th Annual International Conference of the IEEE Engineering in Medicine and Biology Society (EMBC). IEEE; 2013:5606–5609.
17. Kwak NS, Müller KR, Lee SW. A lower limb exoskeleton control system based on steady state visual evoked potentials. J Neural Eng. 2015;12(5):056009.
18. Do AH, Wang PT, King CE, Schombs A, Cramer SC, Nenadic Z. Brain-computer interface controlled functional electrical stimulation device for foot drop due to stroke. Conf Proc IEEE Eng Med Biol Soc. 2012;2012:6414–6417.
19. King CE, Wang PT, McCrimmon CM, Chou CCY, Do AH, Nenadic Z. The feasibility of a brain-computer interface functional electrical stimulation system for the restoration of overground walking after paraplegia. J Neuroeng Rehabil. 2015;12(1):80.
20. Selfslagh A, Shokur S, Campos DSF, Donati ARC, Almeida S, Yamauti SY, et al. Non-invasive, brain-controlled functional electrical stimulation for locomotion rehabilitation in individuals with paraplegia. Sci Rep. 2019;9(1):1–17.
21. López-Larraz E, Trincado-Alonso F, Rajasekaran V, Pérez-Nombela S, Del-Ama AJ, Aranda J, et al. Control of an ambulatory exoskeleton with a brain-machine interface for spinal cord injury gait rehabilitation. Front Neurosci. 2016;10:359.
22. Watanabe T, Murakami T, Handa Y. Preliminary tests of a prototype FES control system for cycling wheelchair rehabilitation. In: 2013 IEEE 13th International Conference on Rehabilitation Robotics (ICORR). IEEE; 2013. p. 1–6.
23. Huang G, Zhang W, Yu Z, Chen X, Meng F, Ceccarelli M, et al. Design and simulation of leg exoskeleton cycling-actuated wheelchair. Int J Adv Robot Syst. 2017;14(6):1-11.
24. Brown DA, Nagpal S, Chi S. Limb-loaded cycling program for locomotor intervention following stroke. Phys Ther. 2005;85(2):159–168.
25. Kautz SA, Brown DA. Relationships between timing of muscle excitation and impaired motor performance during cyclical lower extremity movement in post-stroke hemiplegia. Brain. 1998;121(3):515–526.
26. Muralidharan A, Chae J, Taylor DM. Extracting attempted hand movements from eegs in people with complete hand paralysis following stroke. Front Neurosci. 2011;5(MAR):1–7.
27. Pfurtscheller G, Lopes da Silva FH. Event-related EEG/MEG synchronization and desynchronization: basic principles. Clin Neurophysiol. 1999;110(11):1842–1857.
28. Takahashi M, Takeda K, Otaka Y, Osu R, Hanakawa T, Gouko M, et al. Event related desynchronization-modulated functional electrical stimulation system for stroke rehabilitation: A feasibility study. J Neuroeng Rehabil. 2012;9(1):56.

29. Nolan H, Whelan R, Reilly RB. FASTER: Fully Automated Statistical Thresholding for EEG artifact Rejection. J Neurosci Methods. 2010;192(1).
30. Junghöfer M, Elbert T, Tucker DM, Rockstroh B. Statistical control of artifacts in dense array EEG/MEG studies. Psychophysiology. 2000;37(4).
31. Dhindsa K. Filter-Bank Artifact Rejection: High performance real-time single-channel artifact detection for EEG. Biomed Signal Process Control. 2017;38.
32. Fitzgibbon SP, DeLosAngeles D, Lewis TW, Powers DMW, Grummett TS, Whitham EM, et al. Automatic determination of EMG-contaminated components and validation of independent component analysis using EEG during pharmacologic paralysis. Clin Neurophysiol. 2016;127(3):1781–93.
33. Binnie CD, Cooper R, Mauguiere F, Osselton JW, Prior PF, Tedman BM. Clinical Neurophysiology, Vol. 2 EEG, Paediatric Neurophysiology, Special Techniques and Applications. 1st ed. Elsevier; 2003. p. 1028.
34. Offner FF. The EEG as potential mapping: The value of the average monopolar reference. Electroencephalogr Clin Neurophysiol. 1950;2(1–4):213–214.
35. Ludwig KA, Miriani RM, Langhals NB, Joseph MD, Anderson DJ, Kipke DR. Using a common average reference to improve cortical neuron recordings from microelectrode arrays. J Neurophysiol. 2009;101(3):1679–1689.
36. Murakami M, Nakatani S, Araki N, Konishi Y, Mabuchi K. Motion Discrimination from EEG using logistic regression and schmitt-trigger-type threshold. In: Proceedings - 2015 IEEE International Conference on Systems, Man, and Cybernetics, SMC 2015. pp. 2338-2342.
37. Wang PT, King CE, Chui LA, Do AH, Nenadic Z. Self-paced brain–computer interface control of ambulation in a virtual reality environment. J Neural Eng. 2012;9(5):056016.
38. Farrer C, Valentin G, Hupé JM. The time windows of the sense of agency. Conscious Cogn. 2013;22(4):1431–1441.
39. Menzer F, Brooks A, Halje P, Faller C, Vetterli M, Blanke O. Feeling in control of your footsteps: Conscious gait monitoring and the auditory consequences of footsteps. Cogn Neurosci. 2010;1(3):184–192.
40. Crone NE, Miglioretti DL, Gordon B, Lesser RP. Functional mapping of human sensorimotor cortex with electrocorticographic spectral analysis. II. Event-related synchronization in the gamma band. Brain. 1998;121:2301–15.
41. Brinkman L, Stolk A, Dijkerman HC, de Lange FP, Toni I. Distinct Roles for Alpha- and Beta-Band Oscillations during Mental Simulation of Goal-Directed Actions. J Neurosci. 2014;34(44):14783–14792.
42. Bhattacharyya S, Shimoda S, Hayashibe M. A Synergetic Brain-Machine Interfacing Paradigm for Multi-DOF Robot Control. IEEE Trans Syst Man, Cybern Syst. 2016;46(7):957–968.
43. Krachunov S, Casson A. 3D Printed Dry EEG Electrodes. Sensors. 2016;16(10):1635.
44. Higashi Y, Yokota Y, Naruse Y. Signal correlation between wet and original dry electrodes in electroencephalogram according to the contact impedance of dry electrodes. In: 2017 39th Annual International Conference of the IEEE Engineering in Medicine and Biology Society (EMBC). IEEE; 2017. p. 1062–1065.
45. Arai M, Kudo Y, Miki N. Electroencephalogram measurement from the hairy part of the scalp using polymer-based dry microneedle electrodes. In: 2015 37th Annual

International Conference of the IEEE Engineering in Medicine and Biology Society (EMBC). IEEE; 2015. p. 3165–3168.
46. Kimura M, Nakatani S, Nishida S-I, Taketoshi D, Araki N. 3D Printable Dry EEG Electrodes with Coiled-Spring Prongs. Sensors. 2020; 20(17):4733.
47. Ismail MAF, Shimada S. “Robot” hand illusion under delayed visual feedback: Relationship between the senses of ownership and agency. PLoS One. 2016;11(7).

## Supplemental materials

Beta ERD was used to detect motor intention in our experiment. The learning effect of mu ERD is well known, and several training methods are proposed in this context, such as the basket paradigm (1). Conversely, the cortical 15–25 Hz band (beta) rhythm is said to be similar to the EMG of the muscles (2). However, it is unclear that the intensity of the beta rhythm is promoted by the training. In this supplement, the learning effect was evaluated in our experiment. Healthy 23, 22, and 63-year-old (Sub App A, App B, and App C) participants were enrolled in this experiment. The EEG measurement settings were the same as the main paper. One-way ANOVA tests were used to determine if the error rate and delay time were significantly different between day one and day two. Statistical significance was defined as $p < 0.05$, which corresponded to $F > 3.44$.

First, we compared the error rates between different days. Figure S1 shows the error rate of the same participants on day one and day two. The error rate on day one was significantly higher than that on day two in App A ($F(1,7) = 6.66$, $p < 0.05$), but in App C, the error rate on day one was significantly lower than that on day two ($F(1,7) = 56.6$, $p < 0.001$). In-App B and P1, there were no significant differences. These results did not show significant changes that would be considered common to the different participants.

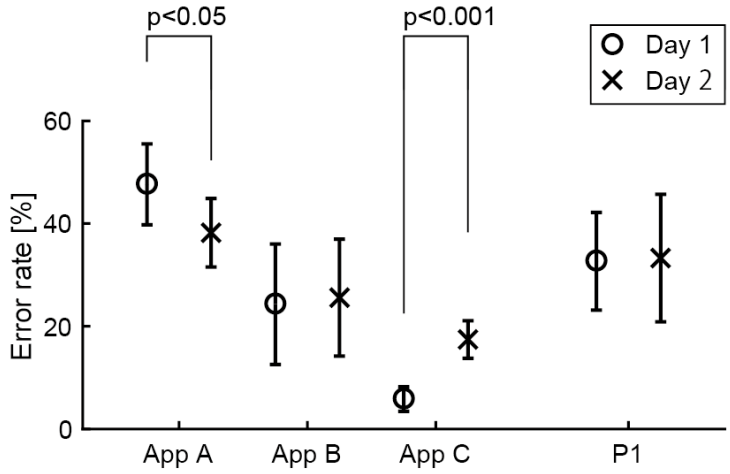


**Figure S1. Mean of error rates among days for healthy participants (App A–C) and the patient with SCI (P1).**

Figure S2 shows the mean error rates and delay times for the three healthy subjects at m = 0, 1, 2, …, and 6. The horizontal axis shows the delay time, and the vertical axis shows the error rate. The plot of day

one indicates “o,” and on the second day, it shows “x.” There were no significant differences in this result, but the error rates and delay times on the second day were not better compared with those on the first day.

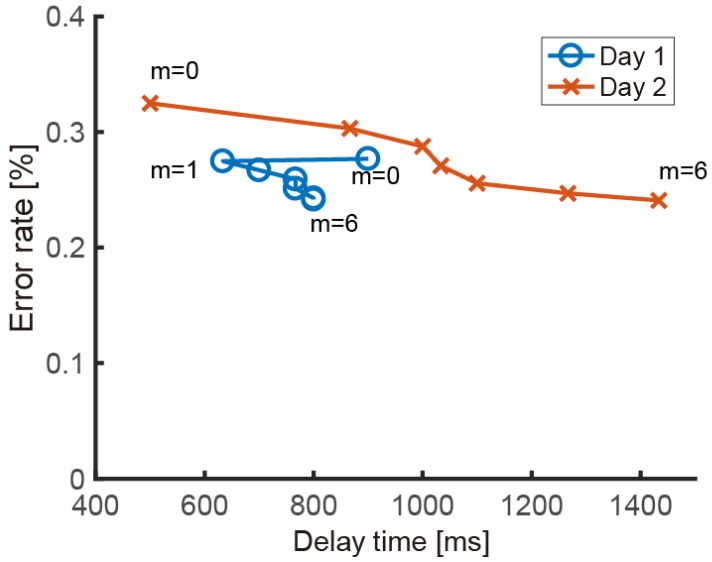


**Figure S2. The relationships between the error-rate mean and the mean of delay time for three healthy participants.**

Finally, we compared the error rates and delay times over a period of five days. Figure S3 shows the relationship between error rates and the delay time of App A during these five days. Parameter m was selected by the proposed method. This result shows that the lowest error rate and the shortest delay time occurred on the third day, and the learning effect is not shown in this figure.

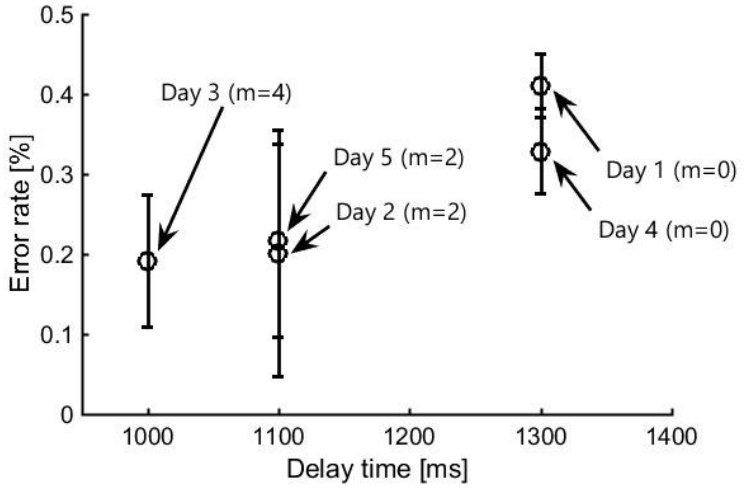


**Figure S3. Mean of the delay times over five days with selected parameter m.**

**Reference**

1. Krausz G, Scherer R, Korisek G, Pfurtscheller G. Critical Decision-Speed and Information Transfer in the "Graz Brain–Computer Interface." Appl Psychophysiol Biofeedback. 2003;28(3):233–40.

2. Brinkman L, Stolk A, Dijkerman HC, de Lange FP, Toni I. Distinct Roles for Alpha- and Beta-Band Oscillations during Mental Simulation of Goal-Directed Actions. J Neurosci. 2014;34(44):14783–92.